Journal of the Serbian Chemical Society
JSCS-info@shd.org.rs • www.shd.org.rs/JSCS
J. Serb. Chem. Soc. *86* (2) 181–194 (2021)
JSCS–5414
Original scientific paper

Folic acid conjugation of magnetite nanoparticles using pulsed electrohydraulic discharges

VLADIMER MIKELASHVILI[1]*, SHALVA KEKUTIA[1], JANO MARKHULIA[1], LIANA SANEBLIDZE[1], ZAUR JABUA[2], LÁSZLÓ ALMÁSY[3] and MANFRED KRIECHBAUM[4]

[1]Vladimir Chavchanidze Institute of Cybernetics of the Georgian Technical University, Z. Anjafaridze str. 5, Tbilisi, 0186, Georgia, [2]Georgian Technical University, Kostava str. 77, Tbilisi 0160, Georgia, [3]Institute for Energy Security and Environmental Safety, Centre for Energy Research, Konkoly Thege str. 29–33, Budapest-1121, Hungary and [4]Institute of Inorganic Chemistry, Graz University of Technology, Stremayrgasse 9/5, A-8010 Graz, Austria

(Received 11 April, revised 2 September, accepted 5 September 2020)

Abstract: The sonochemical coprecipitation reaction with moderate ultrasound irradiation in a low vacuum environment was used to obtain aqueous colloidal suspensions of iron oxide nanoparticles (IONPs). The synthesized magnetite nanoparticles were conjugated directly by folic acid using electrohydraulic discharges as a processing technique before modification of the surface of the nanoparticles. Electrohydraulic discharges were applied in two operational modes with high and low power pulsed direct currents between the electrodes. The physical and chemical properties of the obtained samples were studied using X-ray powder diffraction (XRD), Fourier transform infrared spectroscopy (FTIR), dynamic light scattering (DLS) and small angle X-ray scattering (SAXS). The investigation proved an inverse cubic spinel structure of magnetite with folic acid attachment to the magnetite surface (mean crystallite diameter in the samples, *D*, ranges 25–31 nm by XRD and SAXS). It was found that the processing with electrohydraulic discharges increased the colloidal stability of the folic acid-magnetite nanoparticle dispersions.

Keywords: iron oxide nanoparticles; sonochemical coprecipitation; pulsed arc discharge; surface functionalization.

INTRODUCTION

High-voltage pulsed discharge (HVPD) into a liquid medium is an efficient method used in plasma science and technology. The interaction of non-equilibrium plasma (where the temperature of the ions is much less than that of the electrons $T_e >> T_{ions}$ depending on the energy and discharge type) with a liquid medium finds many important applications in the area of mechanical processing,

* Corresponding author. E-mail: vmikelashvili@gtu.ge
https://doi.org/10.2298/JSC200414053M

fracturing technology in mining,[1] environmental remediation,[2] production of nanomaterials and health care.[3–5] During pulsed electrohydraulic discharges (PEHD) the released electrical energy is converted to mechanical energy. Moreover, different physical and chemical phenomena occur during discharge, such as heat emission, shock wave formation, ultraviolet/visible radiation, the formation of chemically active species ($O^{\bullet}$, $H^{\bullet}$, $^{\bullet}OH$, $HO_2^{\bullet}$), ions (O^-, H^+, H_3O^+) and molecular species (O_2, O_3, H_2, H_2O_2) that either recombine to form stable by-products or return to a lower energetic state emitting in the ultraviolet (UV) range.[6–8]

In recent years, among the variety of discharge types, underwater spark discharges were intensively used in the low-cost production of nanoparticles (NPs) in solution. Although many experimental setups for nanoparticle production have been reported exploring variation of discharging type,[3] parameters (voltage, current), electrode material and configuration, *etc.*, there are very few reports about the processing of the chemically synthesized surface of nanomaterial by high-voltage pulsed arc electrohydraulic discharge for deagglomeration,[9] and further modification of the bare surface of nanoparticles by bioactive molecules for medical application.

Nowadays, the use of iron oxide nanoparticles (IONPs) in diagnostics and therapy is one of the modern strategies in nanomedicine. Magnetic nanocolloids containing IONPs of magnetite (Fe_3O_4) and maghemite (γ-Fe_2O_3) are promising and popular biomedical materials due to their unique magnetic properties. Magnetite exhibits antibacterial activity due to the reactive oxygen species (ROS) generated by Fe_3O_4 NPs, they are hydrophilic and biocompatible. They can be encapsulated with a suitable coating substance for biomedical applications.[10–12]

The most common and cost-effective method for obtaining IONPs is chemical co-precipitation. Although this method is relatively simple, it is necessary to develop an effective strategy to improve the precise control of the main properties of the NPs, such as size, shape, stability, reproducibility and dispersibility of NPs in desired solvents, for bioapplications.[13] The bare iron oxide NPs have high chemical activity and are easily oxidized in air (especially magnetite).[14] Therefore, providing a proper surface coating and developing effective protection strategies to maintain the stability of magnetic iron oxide NPs are important directions of current research.

The method of conjugating folic acid as a specific targeting molecule to magnetite particle is the key to the successful application of magnetic nanoparticles (MNPs) in targeted drug delivery for cancer treatment. Numerous attempts have been made to develop therapeutic drug delivery systems to synthesize folic acid-linked nanoparticle components using surface activation of IONPs with functional molecules, such as chitosan,[15] poly(ethylene glycol),[16,17] poly(ethyleneimine) (PEI),[18] carbodiimide,[19] carboxymethyl dextran,[20] serum folate-bind-

ing protein,[21] which increase their specific uptake by the tumor and inhibit cell growth in microbes and cancer. FA are forms of a water-soluble B_9 vitamin which is a stable, non-immunogenic and low-cost apart from protein-targeting molecules, such as antibodies.

In this paper, continuing previous works,[22–24] a facile method is reported to directly conjugate folic acid (FA) molecules to iron oxide nanoparticles using surface activation with PEHD after their synthesis using *in situ* sonochemical coprecipitation in a low vacuum environment.

EXPERIMENTAL

Chemicals

All chemicals were of analytical grade and used without further purification. Chemicals used for the synthesis of magnetite nanoparticles: ferric chloride hexahydrate ($FeCl_3 \cdot 6H_2O$) (≥98 %), ferrous sulfate heptahydrate ($FeSO_4 \cdot 7H_2O$), ammonium hydroxide solution (NH_4OH, 25 % of NH_3 basis), and folic acid ($C_{19}H_{19}N_7O_6$) (water content (by Karl Fischer) – 9 %, purity (HPLC) >97 %) were purchased from Sigma–Aldrich.

Synthesis of bare magnetic nanoparticles

Bare iron oxide (Fe_3O_4) nanoparticles were prepared by sonochemical coprecipitation with moderate ultrasound irradiation using an iron salt ratio Fe^{3+}/Fe^{2+} of 1.9. First, $FeCl_3 \cdot 6H_2O$ (9 g) + 333 ml distilled water (DW) (0.1 M solution) was prepared in the jacketed reactor 1 (see Fig. 1, temperature 45 °C, mixing duration 20 min, vacuum environment), and $FeSO_4 \cdot 7H_2O$ (4.87 g) +175 ml DW (0.1 M solution) – in the jacketed ultrasonic reactor 2 (temperature 45 °C, duration 20 min, ultrasonication 30 % of 900 W homogenizer, pulse on 2 s, pulse off 1 s).

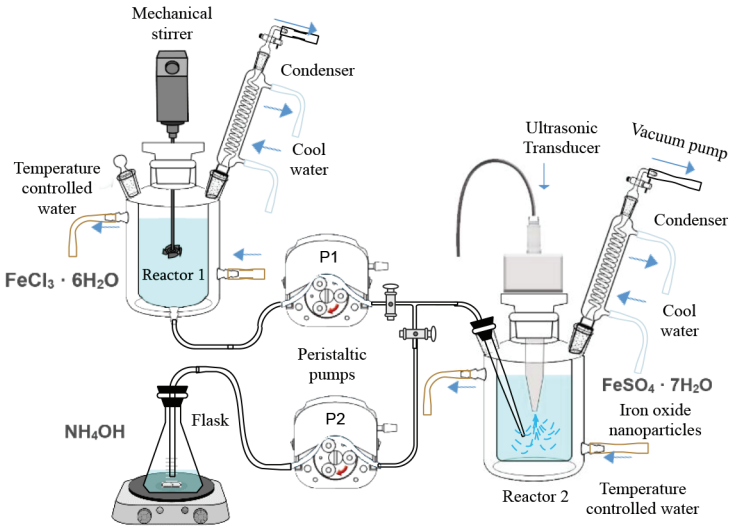

Fig. 1. Experimental set-up for the sonochemical coprecipitation reaction of IONPs with moderate ultrasound treatment in a low vacuum environment.

After dissolution, the iron salt solutions were passed by a peristaltic pump (P1) into the ultrasonic reactor (reactor 2), followed by further sonication. Then, a previously prepared 19 ml NH_4OH (25 %) + 35 ml DW (4 M solution) was added dropwise over 20 min at 45 °C in the middle area of reactor 2 using peristaltic pump P2 (see Fig. 1).

After the formation of the black precipitate, the obtained colloidal suspension was further sonicated for 30 min and gradually cooled to room temperature. This procedure resulted in 570 ml of a black suspension. This fluid was washed several times with an abundant quantity of DW with magnetic separation with a permanent magnet to reduce the pH to the physiological value (initial pH 12, after washing – pH 7.3) and remove the residues of the chemical synthesis. For each sample, 100 ml of the suspension was taken for the preparation of bare IONPs (sample: Bare-IONPs), FA-modified IONPs without PEHD processing (sample: IONPs-FA), FA-IONPs after PEHD processing in two operation modes (see description below) called IONPs-HC-FA and IONPs-LC-FA, respectively.

Electrohydraulic processing

A scheme of the electrohydraulic device is shown in Fig. 2.

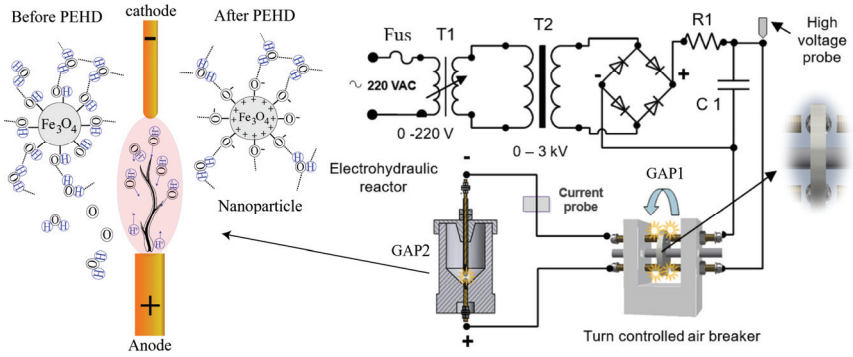

Fig. 2. Electrohydraulic device scheme.

Electrohydraulic processing of 100 ml suspension containing IONPs was performed in a 300 ml volume reactor in a low vacuum. The entire fluid was processed for 5 min. Brass electrodes were immersed through the suspension in the middle of the discharge reactor.

The high voltage transformer T2 has maximum regulated voltage of 3 kV. After that alternating current is transformed to direct current by a diode bridge. The charge accumulated by the capacitor (C1) is transferred through an air gap (Gap 1) that regulates the discharge frequency (by rotating wheel controlled by motor) to the main discharge gap (Gap 2). A digital oscilloscope (Rigol DS1204B) monitors the discharge voltage (voltage transformer: Caltest CT4026) and current (current transformer: Ionphysics CM-01-L).

This device with controlled parameters allows the nanofluid to be processed in two modes:

1. High current (HC) mode (Fig. 3) – the distance between rods, $d = 0.7$ mm, discharge current, $A_{max} = 30$ A, voltage, $V = 1.3$ kV, frequency, $f = 2$ Hz, duration, $t_{max} = 20$ ms;
2. Low current (LC) mode – $d = 2$ mm, $A_{max} = 10$ A, $V = 1.6$ kV, $f = 2$ Hz, $t_{max} = 20$ ms.

The development of a spark discharge in time occurs by successive "germination" of streamers in the interelectrode gap (Fig. 2, GAP2) in which two types of ions (H^+ and OH^-) play the main role. A negative charge accumulated between the electrodes from OH^- dissolve into the liquid, which easily gives off its electrons to the growing streamer channel and form

hydrated electrons (e_{aq}). The hydrated electrons have high reduction potential and induce H^+ reduction at the anode with H_2O and OH^- generation through electrolysis of water at the cathode, respectively, contributing to an increase in the pH value (Fig. 4):[1,7,8]

$$e \rightarrow e_{aq};\ e_{aq} + H_2O_{aq} \rightarrow H_{aq} + OH_{aq}^-;\ e_{aq} + H_{aq}^+ \rightarrow H_{aq}$$

Discharges in water enhance the deprotonation reactions of suspended magnetic nanoparticles as their surface presents amphoteric behaviour:[25,26]

$$\equiv MOH + OH^- \rightarrow \equiv MO^- + H_2O$$

where M is the metal on the surface.

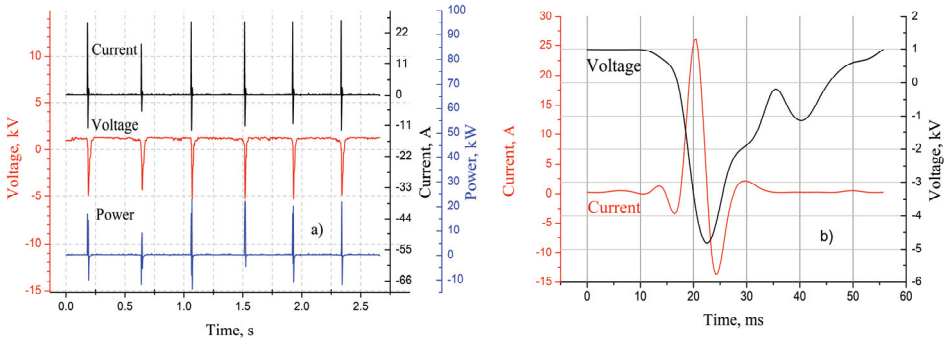

Fig. 3. PEHD in HC mode. a) HC discharge set in 2.5 s; b) one discharge in HC mode.

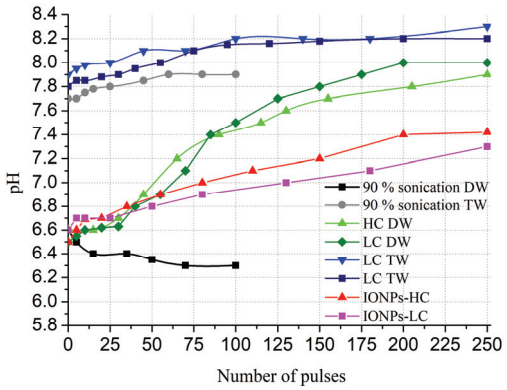

Fig. 4. Comparison of change in pH during electrohydraulic discharge and ultrasonic processing. TW – tap water, DW – distilled water.

Accumulation of the superficial charge on the surface of nanoparticles (see Fig. 2) is due to the specific adsorption of ions (in the present case, Fe ions etching metals during discharge between brass electrodes) during pulsed discharge into water. If the pH is greater than the characteristic point of zero charge (concentrations of positive and negative sites are equal), the discharge develops a negative charge on the nanoparticle surface.

When the streamer passes through the liquid (in the present case, through water), the liquid ions, discharging onto a growing streamer as a "pull-out" electrode, form a thin gas cavity on its surface, which separates the already formed branch of the streamer from the surrounding liquid. The insulating cavity is formed by atomic and molecular oxygen and hydro-

gen, gaseous hydrogen peroxide, as well as electrically neutral free radicals H, OH, existing in the water vapor. Fluid molecules gaining acceleration from the discharge channel, move from discharge zone in all directions, forming a cavitation zone causing the first (main) shock wave. Then the cavity closes at high speed, creating a second spark discharge at given pulse parameters. A sharp increase in the channel temperature and sharp pressure jump induce additional decomposition/deagglomeration products in the liquid inside the channel.

Modification by folic acid

For direct modification (sample IONPs-FA), 100 ml washed precipitate sonicated for 10 min at 30 % energy (900 W, pulse – 2 s, on, 1 s, off) was taken. For 100 ml of suspension, 0.178 g of FA was taken. Previously, FA in 10 ml DW was stirred at 30 °C for 15 min and added by the peristaltic pump to the magnetic fluid and sonicated at 14 % power for 20 min at 30 °C (Fig. 1). After one day, the sample was washed by decanting and separation by a permanent magnet. The pH was increased to 7.4 by dropwise addition of NH_4OH (initial pH was 5.2) diluted in DW, and finally, centrifuged at 4000 rpm during 10 min. The same procedure was applied to the PEHD processed samples. To obtain IONPs-HC-FA and IONPs-LC-FA samples, the initial 2×100 ml of washed and sonicated suspension was processed separately by HC and LC - mode for 5 min each under vacuum and modified directly with FA (as described for sample IONPs-FA).

RESULTS AND DISCUSSION

X-Ray diffraction (XRD)

The phase purity and crystal structure of the synthesized materials were identified *via* XRD analysis (Fig. 5) using a DRON 3M X-ray diffractometer, operating with CuK_α radiation (λ = 1.541 Å) filtered by a nickel foil, voltage – 40 kV, current 20 mA, and scanning speed 2°/min. The diffraction peaks at 2θ values of 30.56, 35.86, 43.46, 54.01, 57.38 and 63.00° were assigned to the crystal planes (220), (311), (400), (422), (511) and (440), respectively. All peaks match well with characteristic peaks of magnetite (Fe_3O_4) (JCPDS file No. 19-0629).

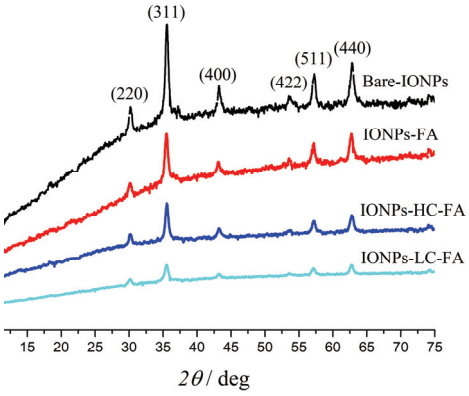

Fig. 5. XRD patterns of synthesized bare--IONPs, bare-IONPs conjugated directly by FA, bare-IONPs processed in the HC and LC mode and conjugated by FA after processing (IONPs-LC-FA and IONPs-LC-FA, respectively).

The X-ray diffraction pattern showed that the materials were crystalline, and no impurity peaks were observed. The average crystallite diameter (D = 28±2

nm) was calculated using the Scherrer Equation from the FWHM of the (311) peak at $2\theta = 35.86°$. The average value of the lattice parameter was found to be $a = 8.37$ Å. Although the presence of maghemite could not be excluded from the diffraction data, the black color of the suspensions and the large lattice parameter indicate a majority of magnetite phase in the prepared nanoparticles.

Fourier-transform infrared spectroscopy (FTIR)

In order to determine the functional groups on the surface of the obtained IONPs, FTIR analysis was performed using an Agilent Cary 670 (Mid-IR spectral range: 5000–400 cm^{-1}) on powder samples after drying in vacuum. The absorption bands of the synthesized iron oxide-NPs (Bare-IONPs) were observed at 3447, 1630, 895, 798 and 578 cm^{-1} (Fig. 6). The peak located at 578 cm^{-1} is associated with the stretching vibration mode of Fe–O characteristic for the magnetite NPs, while the absorption bands at 3447 cm^{-1} indicated the O–H stretching vibration, because the surfaces MNPs are covered with OH groups, as a result of the chemical co-precipitation. The H–O–H deformation peaks at 1630 cm^{-1} (for bare magnetite and also other samples) prove the presence of water adsorbed on the surface of the nanoparticles.[27,28] Comparing the spectrum of bare IONP with folic acid - conjugated IONP, it could be seen that several peaks appeared in the range of 1600–1100 cm^{-1} for the conjugated samples (Fig. 6c–e). These bands are attributed to carboxylic group (C=O) group vibrations of folic acid in the FA--conjugated samples (especially Fig. 6e), indicating FA attachment to the NP surface.

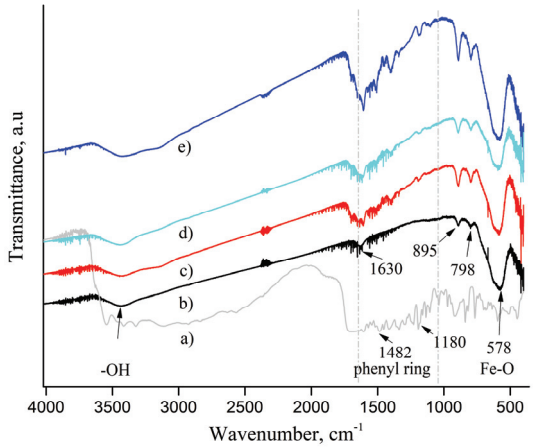

Fig. 6. FTIR spectra of FA (a), bare--IONPs (b), IONPs-FA (c), IONPs--LC-FA (d) and IONPs-HC-FA (e) samples.

Dynamic light scattering (DLS) and zeta potential

In order to determine the hydrodynamic size (D_{hyd}) distribution profile of primary nanoparticles and their aggregates in suspension, an Anton Paar Lite-

sizer™ 500 equipped with a 658-nm laser was used at 25 °C in the back scattering geometry. The refractive indices (*RI*) for the investigated particles (Fe_3O_4 phase) was set to $n = 2.3636$ and $n = 1.3310$ was set for the solvent (distilled water). For an assessment of the stability of the colloidal dispersions and thus the strength of electrostatic repulsion between similarly charged particles, the zeta potential (ζ) of the aqueous suspensions was measured using the same instrument with a scattering angle of 173° at 25 °C and adjusted voltage 200 V. As expected, bare uncovered IONPs possess high hydrodynamic diameter and smaller magnitude of the zeta potential because of the stronger agglomeration. All FA-conjugated samples have the same diameters, although IONPs-FA have a lower zeta potential (19.3 mV) because of partial, insufficient covering.

Small-angle X-ray scattering (SAXS)

The angular distribution of X-rays scattered by the samples injected into quartz capillary at very small (< 10°) angles and at 25 °C was performed on a SAXSpoint 2.0 instrument (Anton Paar GmbH) equipped with a MicroSource, Primux 100 copper X-ray generator (λ = *0*.154 nm) and an Eiger R 1M Tilt 2D detector. In the case of isotropic scattering, the measured intensities are regrouped by radial averaging and presented as the intensity I as a function of momentum transfer or length of the scattering vector q:

$$q = \frac{4\pi \sin\phi}{\lambda} \tag{1}$$

where ϕ is the scattering angle and λ is the wavelength of the X-ray radiation. In order to obtain information of the scattering of the particles only, background subtraction was performed by the ATSAS software (Fig. 7).[29,30]

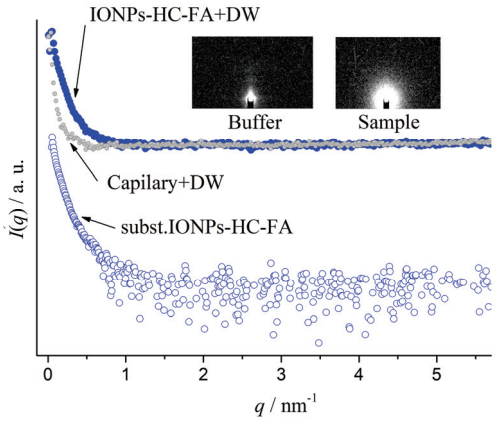

Fig. 7. Experimental image data by a 2D detector (insets) and the circularly averaged scattering curves before and after subtraction of the background scattering. (sample – IONPs-HC-FA diluted in DW) and buffer material (capillary with DW).

One of the most important parameters that provides an estimate of the overall size of a particle (the average electron density-weighted squared distance

to center-of-mass in a particle) is the radius of gyration, R_g (see Fig. 8), which describes the average size of the particles:[31]

$$I(q) = I(0)e^{\frac{-R_g^2 q^2}{3}} \quad (2)$$

where $I(0)$ is forward scattered intensity. The linearity of the Guinier plot (ln I against q^2) is a sensitive indicator of the quality of the experimental data. Deviation from a straight line could indicate aggregation, or a large polydispersity of the scattering particles.

For evaluating the pair distance distribution function $p(r)$ (probable distribution of distances between electrons, Fig. 9), GNOM was used as an indirect Fourier transform program for small-angle scattering data analysis.[32,33]

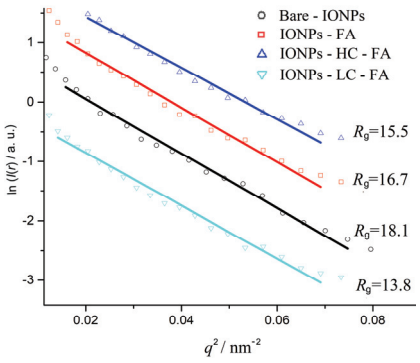

Fig. 8. Guinier plots for evaluating the radius of gyration R_g in the colloid dispersions.

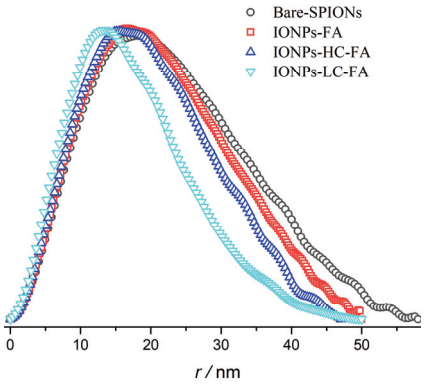

Fig. 9. Pair distribution functions $p(r)$ obtained by GNOM.

Using the output data of GNOM, an *ab initio* shape determination was performed using the bead-modeling program DAMMIF.[32] Starting from an arbitrary initial model, DAMMIF utilizes simulated annealing to construct a compact interconnected cluster of small spherical beads yielding a calculated scattering curve matching the experimental data. As expected, the reconstructed particle

shapes resemble aggregates of nearly spherical particles, Fig. 10. The IONPs-FA clusters have more irregular shapes, which could be related to the effect of the FA coating on the particle agglomeration process.

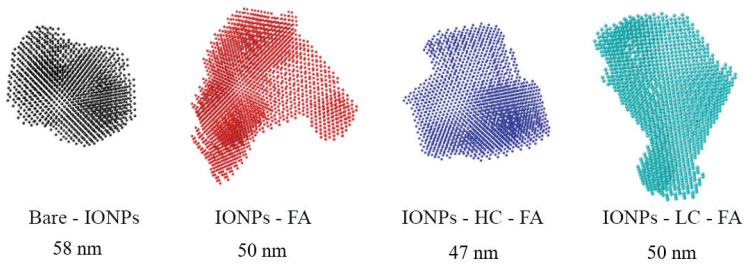

Fig. 10. Bead models of bare and FA-conjugated magnetite clusters containing nanoparticles obtained by the DAMMIF. Numbers in nanometers – maximum cluster diameters (D_{max}).

The scattering curves and subsequent modeling indicate the presence of agglomerates for all the samples.[4,37] Small angle scattering data of agglomerated surfactant-stabilized magnetite nanoparticles in aqueous dispersions are often analyzed using empirical models, such as fractal dependences or the Beaucage model.[36–38]

The assumed-free size distributions of the particles and agglomerates obtained from the scattering patterns by the Monte-Carlo fitting method were evaluated using McSAS software.[39,40] For the Monte Carlo runs, the following parameter values were used: lower and upper q cut-off: 0.05–2.9 nm^{-1}, respectively; number of repetitions 10; model – sphere, distribution of sphere radii between 3–50 nm. The resulting volume-weighted size histograms are shown in Fig. 11, with uncertainties on the bars, and the red dashed line indicating the minimum level required for each bar to contribute in a measurable amount to the scattering pattern (*i.e.*, sensitivity limit).

The obtained distributions are very similar for all the samples, with some variations in the radius range of 20–60 nm, and most of the particles have radii 13–14 nm, which is in good agreement with the single particle or crystallite size obtained from the XRD data.

The analysis results are collected in Table I. The size distribution as given by McSAS analysis reveals two populations, the single nanoparticles, with mean diameter of 22 nm, and the agglomerates with a size distribution from 40 to 100 nm in diameter, with different cluster diameters D_{max} (Fig. 10).

The mechanism of FA conjugation depends on high values of surface charge density of the water-based iron oxide colloids, the pH of the medium, and the ionic strength of the dispersion. In addition, the presence of specific ions (also, the etching particles from brass electrodes in the HC-mode consisting of zinc and copper) at the solid–liquid interface can induce the formation of chemical bonds

favorable for FA conjugation in addition to the pure Coulombic attraction. This interaction is quite probable due also to the fact that FA interacts with the negative charge of the magnetite surface at increased pH values. Comparing dried powder samples of the same mass, the higher intensities of the FA characteristic peaks show that the sample IONPs-HC-FA has a better coating compared to the sample IONPs-LC-FA, in which the particles are less stable and may agglomerate and flocculate due to the smaller surface charge.

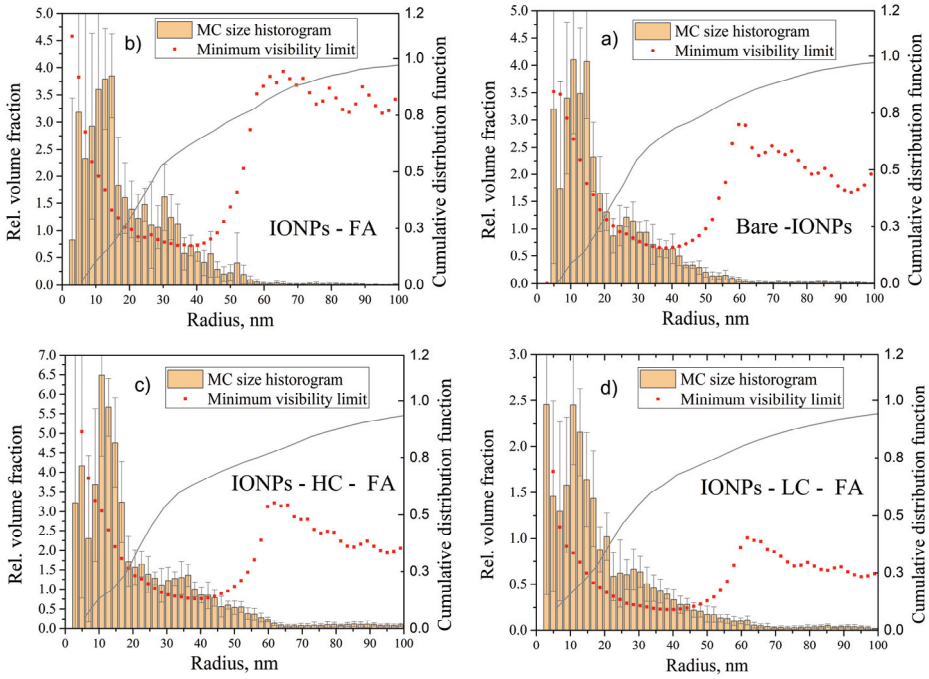

Fig. 11. Particle size distributions obtained using McSAS.

TABLE I. Results of DLS, Zeta potential and SAXS measurements

Material	D_{hyd} / nm	ζ_{mean} / mV	ρ / mS cm^{-1}	R_g[a] / nm	D_{max}[b] / nm	r_{mean}[c] / nm
Bare-IONPs	226.4	21.2	0.019	18.1	58	14
IONPs-FA	141	19.3	0.012	16.7	50	13
IONPs-HC-FA	141.73	25.6	0.013	15.5	47	13.4
IONPs-LC-FA	147.27	24.6	0.038	13.8	50	13.5

[a]Retrieved by PRIMUS; [b]evaluated by DAMMIF; [c]calculated by MsSAS

CONCLUSIONS

A simple, inexpensive and suitable for upscaling technology of preparation of functionalized iron oxide nanoparticles for biomedical use, using non-thermal plasma discharges in water (electrohydraulic discharges) has been developed.

Electrohydraulic discharges assist the modification of MNPs with a bioactive molecule such as folic acid, as proved by FTIR analysis. The presence of specific ions, increased pH and superficial charge around the electohydraulically processed IONPs induce the formation of chemical bonds favorable for FA conjugation in the IONPS-HC-FA dispersions that showed increased zeta potential and stability, compared to the IONPs-LC-FA dispersions and those prepared without electrohydraulic discharges.

Acknowledgements. This research was supported by the Shota Rustaveli National Science Foundation (SRNSF) (grant number: YS17_15) and Central European Research Infrastructure Consortium (CERIC) grant number: 20192124. The authors would like to acknowledge the use of the Somapp Lab, a core facility supported by the Austrian Federal Ministry of Education, Science and Research, the Graz University of Technology, the University of Graz and Anton Paar GmbH.

ИЗВОД

КОНЈУГАЦИЈА МАГНЕТИТНИХ НАНОЧЕСТИЦА ФОЛНОМ КИСЕЛИНОМ КОРИШЋЕЊЕМ ИМПУЛСНИХ ЕЛЕКТРОХИДРАУЛИЧНИХ ПРАЖЊЕЊА

VLADIMER MIKELASHVILI[1], SHALVA KEKUTIA[1], JANO MARKHULIA[1], LIANA SANEBLIDZE[1], ZAUR JABUA[2], LÁSZLÓ ALMÁSY[3] и MANFRED KRIECHBAUM[4]

[1]*Vladimir Chavchanidze Institute of Cybernetics of the Georgian Technical University, Z. Anjafaridze str. 5, Tbilisi, 0186, Georgia,* [2]*Georgian Technical University, Kostava str. 77, Tbilisi 0160, Georgia,* [3]*Institute for Energy Security and Environmental Safety, Centre for Energy Research, Konkoly Thege str. 29–33, Budapest-1121, Hungary u* [4]*Institute of Inorganic Chemistry, Graz University of Technology, Stremayrgasse 9/5, A-8010 Graz, Austria*

Сонохемијска реакција копреципитације са умереним ултразвучним зрачењем у ниском вакууму коришћена је за добијање водених колоидних суспензија наночестица гвожђе-оксида. Синтетизоване наночестице магнетита директно су конјуговане фолном киселином користећи електрохидраулична пражњења као технику обраде пре модификације површине наночестица. Електрохидраулична пражњења примењена су у два оперативна режима са импулсним једносмерним струјама велике и мале снаге између електрода. Физичка и хемијска својства добијених узорака проучавана су применом дифракције рендгенског зрака (XRD), инфрацрвене спектроскопије са Фоуријеовом трансформацијом (FTIR), динамичког расејања светлости (DLS) и рентгенског расејања малих углова (SAXS). Испитивањем је доказана инверзна кубна структура спинела магнетита са везивом фолне киселине на површину магнетита (средњи пречник кристалита, *D*, у узорцима, одређен помоћу XRD и SAXS, је био у опсегу 25–31 nm). Утврђено је да обрада електрохидрауличким пражњењем повећава колоидну стабилност дисперзија наночестица фолне киселине и магнетита.

(Примљено 11. априла, ревидирано 2. септембра, прихваћено 5. септембра 2020)

REFERENCES

1. L. A. Yutkin, *Electro-hydraulic effect and its application in industry*, Engineering, Leningrad, 1986, p. 252 (http://bourabai.ru/library/elektrogidravlicheski_effekt.pdf)
2. E. Leal-Quirós, *Braz. J. Phys.* **34** (2004) 1587 (http://dx.doi.org/10.1590/S0103-97332004000800015)
3. G. Saito, T. Akiyama, *J. Nanomater.* **2015** (2015) 1 (http://dx.doi.org/10.1155/2015/123696)

4. H. Li, K. Wang, X. Tuo, L. Almásy, Q. Tian, G. Sun, M. J. Henderson, Q. Li, A. Wacha, J. Courtois, M. Yan, *Mater. Chem. Phys.* **204** (2018) 236 (http://dx.doi.org/10.1016/j.matchemphys.2017.10.047)
5. S. Horikoshi, N. Serpone, *RSC Adv.* **7** (2017) 47196 (http://dx.doi.org/10.1039/c7ra09600c)
6. Ruma, H. Hosano, T. Sakugawa, H. Akiyama, *Catalysts* **8** (2018) 213 (http://dx.doi.org/10.3390/catal8050213)
7. S. Wakisaka, K. Tsuda, K. Takahashi, K. Satoh, *IEEE Trans. Plasma Sci.* **47** (2019) 1083 (https://doi.org/10.1109/TPS.2018.2866282)
8. H. Shiraishi, G. R. Sunaryo, K. Ishigure, *J. Phys. Chem.* **98** (1994) 5164 (https://doi.org/10.1021/j100070a037)
9. M. I. Lerner, I. A. Gorbikov, O. V. Bakina, S. O. Kasantzev, *Inorg. Mater. Appl. Res.* **8** (2017) 473 (http://dx.doi.org/10.1134/S2075113317030169)
10. P. M. Price, W. E. Mahmoud, A. A. Al-Ghamdi, L. M. Bronstein, *Front. Chem.* **6** (2018) 619 (http://dx.doi.org/10.3389/fchem.2018.00619)
11. T. Vangijzegem, D. Stanicki, S. Laurent, *Expert Opin. Drug Deliv.* **16** (2019) 69 (http://dx.doi.org/10.1080/17425247.2019.1554647)
12. S. Palanisamy, Y. M. Wang, *Dalton Trans.* **48** (2019) 9391 (http://dx.doi.org/10.1039/c9dt00459a)
13. A. Stepanov, R. Mendes, M. Rümmeli, T. Gemming, I. Nizameev, A. Mustafina, *Chem. Pap.* **73** (2019) 2715 (http://dx.doi.org/10.1007/s11696-019-00823-9)
14. A. Ali, H. Zafar, M. Zia, I. ul Haq, A. R. Phull, J. S. Ali, A. Hussain, *Nanotechnol. Sci. Appl.* **9** (2016) 49 (http://dx.doi.org/10.2147/NSA.S99986)
15. H. Arami, Z. Stephen, O. Veiseh, M. Zhang, *Adv. Polym. Sci.* **243** (2011) 163 (http://dx.doi.org/10.1007/12_2011_121)
16. T. Keskin, S. Yalcin, U. Gunduz, *Inorg. Nano-Metal Chem.* **48** (2018) 150 (http://dx.doi.org/10.1080/24701556.2018.1453840)
17. M. Erdem, S. Yalcin, U. Gunduz, *Hum. Exp. Toxicol.* **36** (2017) 833 (http://dx.doi.org/10.1177/0960327116672910)
18. H. Yoo, S. K. Moon, T. Hwang, Y. S. Kim, J. H. Kim, S. W. Choi, J. H. Kim, *Langmuir* **29** (2013) 5962 (http://dx.doi.org/10.1021/la3051302)
19. A. Ancira-Cortez, E. Morales-Avila, B. E. Ocampo-Garciá, C. González-Romero, L. A. Medina, G. López-Téllez, E. Cuevas-Yáñez, *J. Nanomater.* **2017** (2017) 1 (http://dx.doi.org/10.1155/2017/5184167)
20. Q. L. Jiang, S. W. Zheng, R. Y. Hong, S. M. Deng, L. Guo, R. L. Hu, B. Gao, M. Huang, L. F. Cheng, G. H. Liu, Y. Q. Wang, *Appl. Surf. Sci.* **307** (2014) 224 (http://dx.doi.org/10.1016/j.apsusc.2014.04.018)
21. J. Chen, S. Klem, A. K. Jones, B. Orr, M. M. B. Holl, *Bioconjug. Chem.* **28** (2017) 81 (http://dx.doi.org/10.1021/acs.bioconjchem.6b00526)
22. J. Markhulia, V. Mikelashvili, S. Kekutia, L. Saneblidze, Z. Jabua, D. Daraselia, D. Jafaridze, *J. Pharm. Appl. Chem.* **2** (2016) 33 (http://dx.doi.org/10.18576/jpac/020201)
23. J. Markhulia, S. Kekutia, Z. Jabua, V. Mikelashvili, L. Saneblidze, in *Proceedings of* 7th International Multidisciplinary Scientific GeoConference *SGEM 2017,* (2017), Sofia, Bulgaria, *SGEM2017 Conference Proceedings* **17,** SGEM, Sofia, 2017, pp. 51–58 (http://dx.doi.org/10.5593/sgem2017/61/S24.007)
24. J. Markhulia, S. Kekutia, N. Mitskevich, V. Mikelashvili, L. Saneblidze, N. Leladze, Z. Jabua, L. Sacarescu, M. Kriechbaum, L. Almásy, *Dig. J. Nanomater. Biostructures* **13** (2018) 1081 (http://www.chalcogen.ro/1081_MarkhuliaJ.pdf)

25. A. F. C. Campos, W. C. De Medeiros, R. Aquino, J. Depeyrot, *Mater. Res.* **20** (2017) 1729 (http://dx.doi.org/10.1590/1980-5373-MR-2017-0649)
26. E. Illés, E. Tombácz, *J. Colloid Interface Sci.* **295** (2006) 115 (https://doi.org/10.1016/j.jcis.2005.08.003)
27. F. Márquez, G. M. Herrera, T. Campo, M. Cotto, J. Ducongé, J. M. Sanz, E. Elizalde, Ó. Perales, C. Morant, *Nanoscale Res. Lett.* **7** (2012) 210 (http://dx.doi.org/10.1186/1556-276X-7-210)
28. M. Mahdavi, M. Bin Ahmad, M. J. Haron, F. Namvar, B. Nadi, M. Z. Ab Rahman, J. Amin, *Molecules* **18** (2013) 7533 (http://dx.doi.org/10.3390/molecules18077533)
29. D. Franke, M. V. Petoukhov, P. V. Konarev, A. Panjkovich, A. Tuukkanen, H. D. T. Mertens, A. G. Kikhney, N. R. Hajizadeh, J. M. Franklin, C. M. Jeffries, D. I. Svergun, *J. Appl. Crystallogr.* **50** (2017) 1212 (http://dx.doi.org/10.1107/S1600576717007786)
30. P. V. Konarev, V. V. Volkov, A. V. Sokolova, M. H. J. Koch, D. I. Svergun, *J. Appl. Crystallogr.* **36** (2003) 1277 (http://dx.doi.org/10.1107/S0021889803012779)
31. A. Guinier, G. Fournet. *Small-Angle Scattering of X-rays,* Wiley, New York, 1955 (https://pdfs.semanticscholar.org/e307/79ad3cf2fb2e2c0a4d6c6b9f6a92bafec4a8.pdf)
32. A. V. Semenyuk, D. I. Svergun, *J. Appl. Crystallogr.* **24** (1991) 537 (http://dx.doi.org/10.1107/S002188989100081X)
33. D. I. Svergun, *J. Appl. Crystallogr.* **24** (1992) 495 (http://dx.doi.org/10.1107/S0021889892001663)
34. D. Franke, D. I. Svergun, *J. Appl. Crystallogr.* **42** (2009) 342 (http://dx.doi.org/10.1107/S0021889809000338)
35. S. Zhu, Y. Leng, M. Yan, X. Tuo, J. Yang, L. Almásy, Q. Tian, G. Sun, L. Zou, Q. Li, J. Courtois, H. Zhang, *Appl. Surf. Sci.* **447** (2018) 381 (http://dx.doi.org/10.1016/j.apsusc.2018.04.016)
36. D. F. Coral-Coral, J. A. Mera-Córdoba, *DYNA* **86** (2019) 135 (http://dx.doi.org/10.15446/dyna.v86n209.73450)
37. V. I. Petrenko, O. P. Artykulnyi, L. A. Bulavin, L. Almásy, V. M. Garamus, O. I. Ivankov, N. A. Grigoryeva, L. Vekas, P. Kopcansky, M. V. Avdeev, *Colloids Surfaces, A* **541** (2018) 222 (http://dx.doi.org/10.1016/j.colsurfa.2017.03.054)
38. A. Taufiq, Sunaryono, N. Hidayat, A. Hidayat, E. G. R. Putra, A. Okazawa, I. Watanabe, N. Kojima, S. Pratapa, Darminto, *Nano* **12** (2017) 1750110 (http://dx.doi.org/10.1142/S1793292017501107)
39. B. R. Pauw, J. S. Pedersen, S. Tardif, M. Takata, B. B. Iversen, *J. Appl. Crystallogr.* **46** (2013) 365 (http://dx.doi.org/10.1107/S0021889813001295)
40. B. R. Pauw, C. Kästner, A. F. Thünemann, *J. Appl. Crystallogr.* **50** (2017) 1280 (http://dx.doi.org/10.1107/S160057671701010X)